Accurate Thermoreflectance Imaging of Nano-Features Using Thermal Decay

Dustin Kendig[1], Gregory Hohensee[2], Ella Pek[3], Wan Kuang[2], Kazuaki Yazawa[1,4], Ali Shakouri[4]
[1]Microsanj LLC.
[2]Western Digital
[3]University of Illinois at Urbana-Champaign
[4]Purdue University

3287 Kifer Road
Santa Clara, CA, 95051 USA
Email: dustin@microsanj.com

ABSTRACT

Thermal characterization of nano-featured devices is a critical challenge for the development of high performance devices. Although far-field thermoreflectance imaging is limited in spatial resolution by the optical diffraction limit, it is more amenable to absolute temperature calibration of plasmonic devices than existing near-field scanning probe tip methods. We have built an advanced thermoreflectance microscope capable of 50 ns time-resolved, diffraction-limited temperature imaging that can account and correct for thermal expansion, sample drift, numerical aperture, and polarization induced variations in the apparent thermoreflectance coefficient of nanoscale structures. We developed a per-pixel transient calibration technique using this microscope to measure the absolute temperature of an operating heat-assisted magnetic recording (HAMR) head, including features as narrow as 200 nm. The resulting temperature information can be used to experimentally validate numerical models in the design process of such plasmonic devices.

KEY WORDS: thermoreflectance, nanoscale thermal imaging, thermal decay, heat-assisted magnetic recording

NOMENCLATURE

C_{th}	thermoreflectance coefficient
R	reflective intensity, (J/m^2)
T	temperature, (K)
t	time, (s)

Greek symbols

λ	wavelength, (m)

INTRODUCTION

As modern electronics push further into the nanoscale range, the thermal management of peak temperatures in isolated, high power density active nanoscale devices[1,2] is becoming a severe limiter. Computational thermal simulations can still guide design, but thermal imaging techniques that can validate and inform the models are struggling to keep up. As designers push farther into the nanoscale where thermal conductivities deviate from their bulk values, conventional Fourier thermal physics can break down, and thermal boundary conductances become highly relevant and difficult to predict,[3,4,5] the challenge of absolute nanoscale thermometry is becoming more of a bottleneck in keeping computational models grounded.

IR thermal imagers with microscale resolution [6] are not informative at the nanoscale. Single-point (or line) thermistors do not provide much spatial information, generally can't overlap with an active nanoscale device, and require electrical leads that may be impractical in a production device. Scanning thermal microscopy (SThM) [7] has excellent spatial resolution and has recently overcome some important calibration challenges.[8]

However, a radiative or plasmonic device will throw a wrench in any near-field scanning technique: the probe tip will interact with, and be directly heated by, the near- and far-field radiation from the device. This results in a convolution of thermal and optical signals that blocks calibration to absolute temperature. Similarly, nanoparticle thermometers[9] cannot be placed too close to an optical device, or they'll disturb the device's operation and be optically heated as well. This is a challenge for the characterization of heat-assisted magnetic recording (HAMR) heads. HAMR is currently the most promising path forward for increasing areal density (storage capacity) of hard disk drives,[10,11] but the HAMR writer is a nanoscale plasmonic device that must operate at an exceptional optical power density under harsh conditions.[12] HAMR's reliability and future will depend on thermal management, thus viable nanoscale thermometry techniques are needed.

So far, there are only two techniques which show promise in measuring the absolute temperature of a plasmonic device at the sub-100 nm length scale. These are polymer imprint thermal mapping (PITM) [13], and TEM-based energy loss spectroscopy.[14] The first technique is still immature and cumbersome, and the latter is only viable for 2D devices that still operate after TEM sectioning, untested for plasmonic devices, and not very scalable.

Above the 100 nm scale, far-field optical thermometry becomes attractive, and thermoreflectance imaging [15] is the most convenient and sensitive optical method to date. As we demonstrate in this paper, it can obtain time-resolved surface temperature maps for features as narrow as 200 nm. It may lack spatial resolution compared to scanning probe techniques, but absolute temperature calibration is more achievable, since radiation from the plasmonic device can be filtered out.

That said, the calibration of nanoscale thermoreflectance images is complicated by several factors, including (1) sample drift from global thermal expansion at long time scales, (2) local thermal expansion, (3) a strict subpixel image registration requirement for diffraction-limited features, (4) numerical aperture (NA) dependent calibration at high NA,

and (5) polarization-dependent response of nanoscale features. We have developed an advanced thermoreflectance imaging system to explore and manage these issues, and have thereby successfully captured an absolute temperature profile of diffraction-limited features of a plasmonic HAMR head.

TIME-RESOLVED THERMOREFLECTANCE

The present technique is based on transient thermoreflectance imaging. The following section describes the method how the time-resolved thermal images are collected, followed by the analytical modeling and discussion of thermal decay signals.

The complex refractive index of a material changes with temperature, and the thermoreflectance coefficient C_{th} simply represents the linear change in optical reflectance of a surface due to a change in temperature:

$$\frac{\Delta R}{R_0} = C_{th}(\lambda)\Delta T \qquad (1)$$

The thermoreflectance effect is central to pump-probe spectroscopy on metals,[16] including picosecond acoustics for thin-film thickness and mechanical characterization,[17] as well as cutting-edge nanoscale thermal characterization techniques, most notably time-domain thermoreflectance (TDTR).[3]

We use stroboscopic imaging [18] to create time-resolved image data with temporal resolution down to 50 ns. The device is turned ON for a designated period of time at a designated duty cycle, and the CCD exposure time is also set by the user. Nearly all the light reaching the CCD will come from the LED pulses which are offset by a specific time delay relative to the device excitation, and a CCD image is generated as the sum of the LED pulses inside a single CCD exposure window.

To create a transient thermoreflectance image, a reference CCD image with LED pulse delay t = 0 is collected, followed by a t > 0 CCD image; then, a subpixel image registration algorithm is applied to a subset of the CCD images to align the t > 0 image to the reference, after which the registered t > 0 image is subtracted from the t = 0 reference. This process with pairs of t = 0, t > 0 images continues as a running average to suppress noise to an acceptable level. In this way, the software can automatically step through user-designated time delays and averaging times to collect a full time-domain image set, from the moment the device is turned on, to the time period after the device switches off and is cooling down, all without user involvement.

While this is ongoing, the system periodically checks the current reference CCD image against an initial image taken at the start of the measurement. The system can detect Z-axis sample drift by comparing the sharpness of the initial and current images, and detect XY sample drift by image registration. When it detects sample drift relative to the microscope, it controls an underlying 3-axis piezo nano-positioning stage to compensate so that there is no long-term sample drift, even when collecting and averaging data overnight. With the 250x, 0.9NA objective we have 18 nm/pixel. The piezoelectric stage has <1nm positioning resolution, and with a sub-pixel detection between 0.02-0.04, the system can correct for slow (>1s) drifts down to <1nm in the XY-axis. Positioning in the Z-axis is limited by the depth of focus of the objective to ~10 nm. Instantaneous XY shifts due to vibrations or other movements is corrected for digitally in each frame.

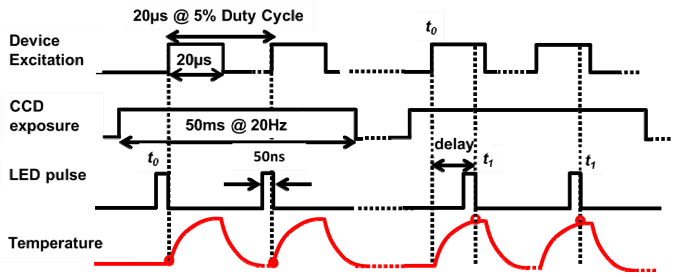

Fig. 1 Timing diagram showing how we collect time-resolved image data by pulsing the device excitation and LED probe light at a controllable relative time delay, essentially like a pump-probe laser system. This diagram shows how the t = 0 data point is collected.

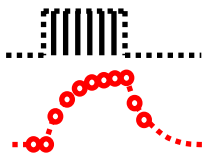

Fig. 2 Inter-locking transient imaging method: Temperature data points are acquired by shifting the timing delay each cycle to achieve a time resolution limited only by how tightly we can pulse the LED probe light.

TCAT: Thermoreflectance Coefficient Analysis Tool

Aside from completely uniform samples, the thermoreflectance image is not a 1:1 map to temperature: different features, and even edges of features, will have different effective thermoreflectance coefficients. For microscale and larger features, a generic hot-plate temperature calibration technique is entirely sufficient. In our system, we place the sample with a thermocouple on a 1 mm tall, 1 cm x 1 cm square Peltier heating stage under the microscope. We then periodically drive the stage to high temperature and back to ambient, and measure the intensity difference between CCD frames in the hot and cold states. All the techniques described above for transient thermal imaging apply, except for TCAT we allow 30-60 seconds per cycle for the stage and sample to reach thermal equilibrium before taking the hot/cold images. The thermoreflectance coefficient is calculated pixel-by-pixel by dividing the change in reflectance by the monitored temperature rise.

In Figure 3, we see that the quality of the resulting thermoreflectance coefficient map depends heavily on how well the system manages thermal expansion induced sample drift and image registration. With a 250x microscope objective, even a modest temperature rise (or return to ambient) will generate a net thermal expansion in the heating stage and sample that far exceeds the depth of focus, so the system must efficiently drive the 3-axis piezo stage to recapture the sample surface and bring it back into alignment before collecting the hot or cold image. Misalignment in X and Y can be corrected for by image registration, but even a

small Z focus misalignment between hot and cold images will generate artifacts. See Refs. [18-19] for implementation details.

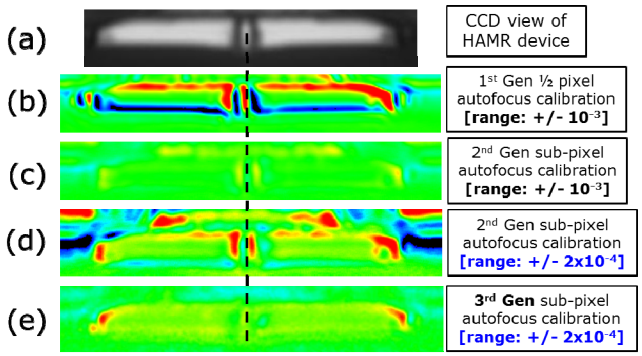

Fig. 3 (a) CCD image of HAMR plasmonic device, featuring two wearpads (approx. 1 micron tall) and a central magnetic write pole (approx. 200 nm wide). The plasmonic near-field transducer (NFT) lies immediately below the write pole, but is smaller than 100 nm and not visible under 530 nm LED illumination. **(b)** TCAT thermoreflectance coefficient map; note the saturated red and blue extremes due to imperfect image registration, and how they overwhelm signal (green) from the pole and edges of the wearpads. **(c)** 2nd generation TCAT map with sub-pixel (to 1/50th of a pixel) image registration, same color scale. **(d)** Same as (c), but reduced scale to show that the true C_{th} (of order 5 x 10^{-5} K^{-1}) is still overwhelmed over the diffraction-limited pole. **(e)** 3rd generation TCAT map, same scale as (d). The symmetry in (e) as opposed to (b) indicates that edge effects are now dominated by global thermal expansion, not image mis-registration. The wearpad C_{th} is easily extracted, and the pole C_{th} looks slightly artificial, but similar in magnitude. This is not surprising, since the wearpads and pole are made of the same material.

Artifacts in TCAT are of two origins. First, Dilhaire et al. discovered that a parasitic Fabry-Perot mode can be generated between a very high NA objective lens and the sample surface, such that the observed reflectance is modulated at a scale shorter than the depth of focus (see [20], Fig. 2). An inconsistency in focal position between hot/cold images can influence the apparent thermoreflectance coefficient, not just near edges.

The second category, edge effects, is most severe for micron and sub-micron features and can arise from poor Z alignment, poor XY image registration, and large scale thermal expansion that slightly changes the size and spacing between features. Figure 3(b) showcases XY image mis-registration artifacts, and 3(e) shows mainly global thermal expansion artifacts, the red patches at the ends of the wearpads. A single nanometer (1/20th of a pixel, here) mis-registration will create major edge effects across the field of view, while global expansion edge effects are magnified away from the reference region for image registration. See the Appendix for more details.

TRANSIENT CALIBRATION

Global thermal expansion artifacts are inevitable so long as the wafer holding the device is heated isothermally. However, if the microscale region containing the device is brought to a local thermal equilibrium without global heating by a heating stage, global thermal expansion artifacts can be minimized by several orders of magnitude. The remaining impact of thermal expansion is strictly local, and cannot be treated as an "artifact" so much as an inherent part of the thermoreflectance response along the diffraction-limited edges of a nano- or micro-scale structure.

One can contemplate this by observing the transient thermoreflectance response of our device in Figure 4b. The NFT is the heat source (red dot), so it is unphysical for the wearpads to be hot, cool, and hot again along the y-axis away from the NFT. It also makes no sense for the wearpad to be rimmed with heat all along the far edges. In fact, the thermoreflectance signal along the edges has two components: a change in refractive index as usual, plus local thermal expansion which increases the size of each feature, which means increased reflectance from the expanded edges.

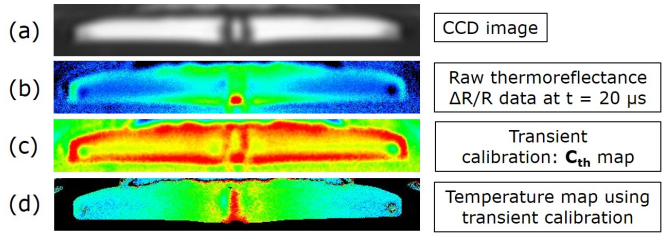

Fig. 4 (a) CCD image of device. **(b)** Transient thermoreflectance image at t = 20 μs, local steady state (see Fig. 5). The enhanced signal along the edges of the wearpad show that a single thermoreflectance coefficient cannot describe this structure. **(c)** True, pixel-by-pixel thermoreflectance coefficient map from the transient calibration technique, showcasing the contribution of local thermal expansion along edges and diffraction-limited features. **(d)** The calibrated temperature map, combining (b) and (c). The temperature map is masked to reject spurious signal from very low C_{th} obtained over non-reflective (low SNR) regions away from the device.

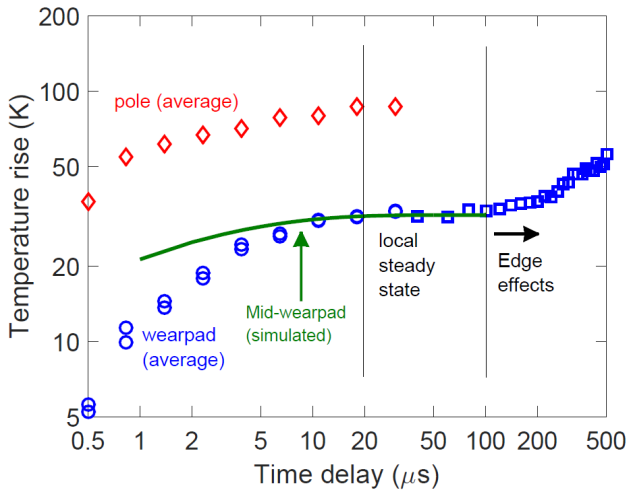

Fig. 5 Demonstration that the HAMR device reaches local thermal equilibrium after 20 μs of excitation. The green curve is a simulated, rescaled temperature rise at the midpoint of the wearpad. The wearpad average data points (blue circles, squares) lag below the simulation because the wearpad average data includes the far ends, which take longer to heat up. The pole average temperature (red diamonds) was determined by an ROI-based transient calibration. Beyond 100 μs, edge-effect artifacts crept into the wearpad region, much like in the TCAT data shown in Fig. 3b. The onset of edge effects would be later in the current version of the system's software.

To demonstrate local thermal expansion, and generate a proper temperature map, we first achieve local thermal equilibrium by powering the device to a local steady-state temperature condition. In Figure 5, we plot the average temperature rise over time of a wearpad interior ROI and a write pole ROI, assuming they have equal thermoreflectance coefficients (as suggested in Fig. 3e). The data and corresponding simulation shown in Figure 5 shows that we can reach local steady-state heating by powering the device for 20 μs.

Next, we collect transient thermoreflectance image data across t = 18 to 27 μs, encompassing the steady-state peak temperature near t = 20 μs, as well as most of the cooling trend after the device is turned off. In Figure 6b, we monitor horizontal cross-sections across both pads and pole out to t = 22 μs, at which time we observe a flat nonzero signal along the interior midline of the wearpads, which we know has uniform thermoreflectance coefficient. This indicates that the HAMR device surface has reached a local thermal equilibrium at an elevated temperature.

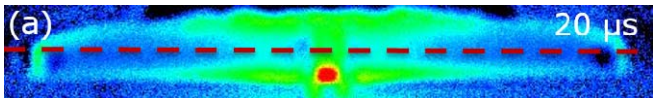

Fig. 6a Raw thermoreflectance signal of device at steady-state operating temperature; red dashed line indicates device midline cross-section, plotted in Fig. 6b (below) over time after power is turned off.

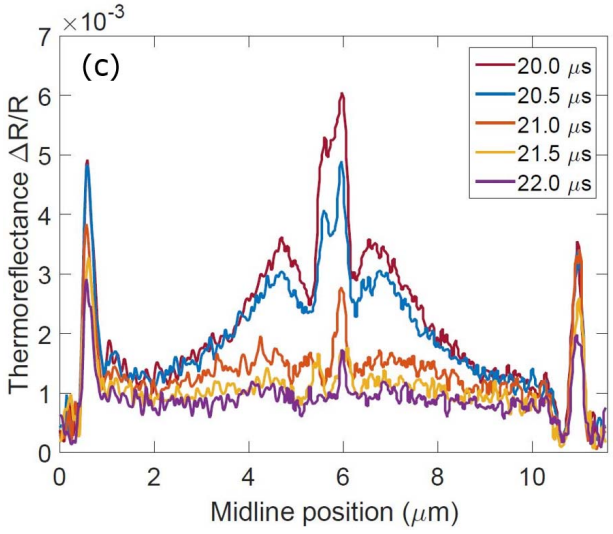

Fig. 6b Mid-line horizontal cross-section of raw thermoreflectance signal over time after device is powered off. The gradient inside the wearpads (uniform thermoreflectance coefficient) goes to zero and the device approaches a local thermal equilibrium at 20 K above room temperature. The sharp peaks are caused by local thermal expansion in addition to thermoreflectance.

Knowing the time of local thermal equilibrium, we apply a new technique that we call "transient calibration (TransientCAL™)." We find the average thermoreflectance signal in a wearpad interior region, and assign it a known thermoreflectance coefficient based on our TCAT data (Fig. 3e). From this reference, we then assign thermoreflectance coefficients on a pixel-by-pixel basis across the whole transient thermoreflectance image (or series of images) at t > 22 μs, on the assertion that the temperature everywhere is equal to the known average wearpad temperature at a given time step. The result is a true thermoreflectance calibration image, as shown in Figure 4c. The enhanced thermoreflectance coefficients along the edges and on diffraction-limited features, including the unresolved NFT at the base of the write pole, are due to local thermal expansion of each structure. Fortunately, the local thermal expansion contributes linearly to the observed change in reflectance signal along all edges in our device (Figure 7c). Essentially, TransientCAL™ is agnostic to the cause of reflectance changes as the device is powered, be it thermoreflectance or thermal expansion, so long as the reflectance changes linearly.

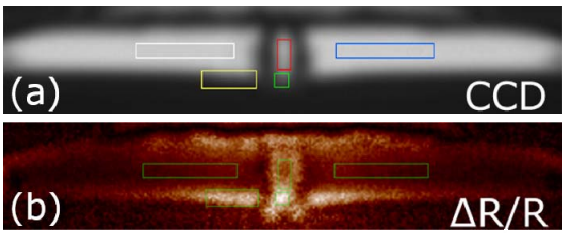

Fig. 7a-b The (a) CCD and (b) raw thermoreflectance ΔR/R images show the color codes and locations of the ROIs where the average signals were taken as a function of laser power in Fig. 7c (below).

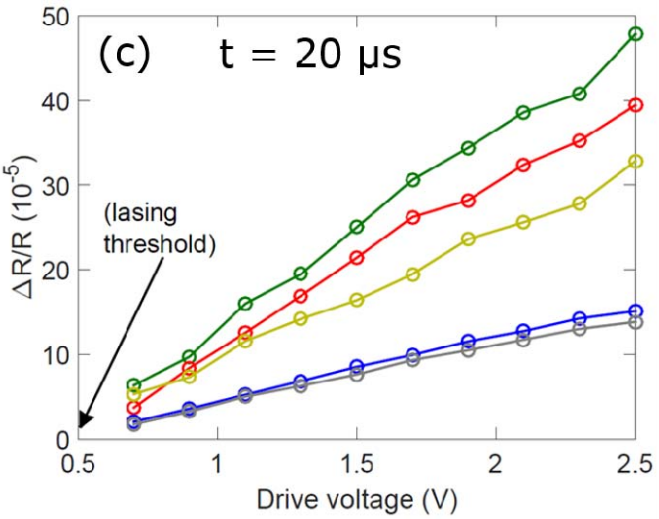

Fig. 7c Raw thermoreflectance ΔR/R signals versus drive voltage (laser power) at various regions of the device, under local steady-state heating. The unresolved NFT (green), under-resolved pole (red), wearpad edges (yellow), and wearpad interiors (blue, gray) all show a linear response up to the maximum laser power. This shows that the local thermal expansion component of the observed ΔR/R is also linear, and therefore can be bundled into an effective thermoreflectance coefficient by the transient calibration technique, as in Fig. 4c.

We can verify that TransientCAL proceeded correctly by plotting the cooling curves for representative regions on the wearpads and pole, and observing that all curves overlap in local thermal equilibrium after a few microseconds, as shown in Figures 8a-c.

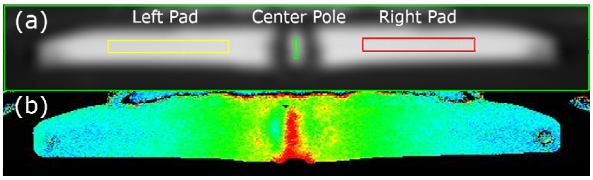

Fig. 8a-b CCD image (a) and transient calibrated temperature map (b) for HAMR device, copied from Fig. 4d. Rectangles in CCD image define regions of interest in which the average temperature is monitored over time and plotted in Fig. 8c (below).

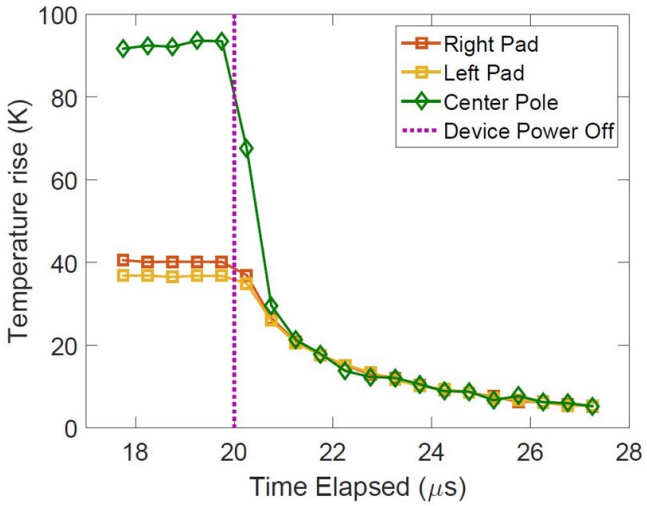

Fig. 8c Cooling curves showing average temperature rises of selected regions (Fig. 8a), from local steady-state heating to +7.5 μs after the power bias is shut off at t = 20 μs (dotted vertical line). In agreement with the uniform wearpad temperature seen after t = 22 μs in Fig. 6b, here we see that the transient-calibrated temperature map shows local thermal equilibrium is reached about 2 μs after the power is shut off.

Polarization-dependence in nanoscale thermoreflectance

We have also observed a plasmonic response in the thermoreflectance images of our HAMR device. This is to be expected, since thermoreflectance is built from the reflectance spectrum, and the reflectance of a structure will deviate from the norm near a plasmon resonance. In particular, a 40 nm Au nanosphere has a plasmon resonance at 530 nm, exactly the illumination wavelength we are using to probe the thermoreflectance of the HAMR device, which contains a similarly sized Au NFT structure.

Specifically, the plasmonic response manifests as a polarization dependence of the thermoreflectance signal. Because the HAMR NFT and surrounding metals have different dimensions along the x- and y-axes of our imaging system, x- and y-polarized light from the microscope's LED will be more or less distant from a plasmon resonance peak, with a corresponding difference in the measured thermoreflectance signal, as observed in Figure 9. Note that our thermoreflectance signal is $\Delta R/R$, not the absolute ΔR, so any differences in illumination intensity or reflectance R between the two polarizations are normalized out.

The important takeaway from the polarization dependence is that the thermoreflectance of a nanoscale structure is intimately tied to its exact shape and dimensions, in addition to the linear thermal expansion coefficient and the wavelength and polarization states of the illuminating light source. Because mass-produced nanoscale devices have dimensional tolerances on the nanoscale as well, we can expect non-trivial differences in thermoreflectance calibrations from device to device. This makes it important to calibrate on a per-device basis. It also makes the transient calibration technique particularly convenient; it can be done in-situ without mounting (with thermal adhesive) on a heating stage, so long as a pre-calibrated microscale reference surface is adjacent to the nanoscale structure of interest.

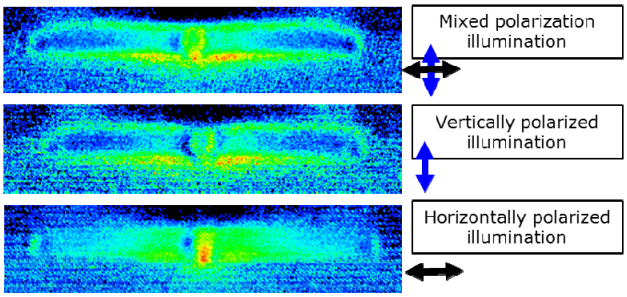

Fig. 9 The observed thermoreflectance signal for three different polarization states of the 530 nm LED probe illumination. This is not the same device or averaging time as for other figures. Vertical and horizontal polarizations were generated by inserting a linear polarizer in front of the LED. The mixed polarization state was just the LED without filters; the horizontal and vertical components were similar but not equal in magnitude. Broadly, the thermoreflectance appears enhanced where the polarization is aligned with the short dimension of a visible structure.

CONCLUSION

Using a prototype HAMR head for next-generation hard disk drives as motivation, we have demonstrated a commercially-available thermoreflectance microscopy system capable of calibrating the absolute temperature rise of a sub-micron plasmonic device down to the optical diffraction limit. This system manages several key difficulties and considerations on the path to calibrating and measuring the time-dependent, absolute temperature rise of structures as narrow as 200 nm. These include sample drift, edge effects, global thermal expansion artifacts, the linear local thermal expansion contribution to thermoreflectance along edges, and the wavelength-, numerical aperture-, and polarization-dependence of nanoscale thermoreflectance signals.

To manage these factors, we developed subpixel image registration, 3-axis sample drift correction, and autofocus algorithms for stable isothermal calibration of single-micron sized structures. In order to achieve diffraction-limited, sub-micron temperature calibration, we developed a transient calibration technique, aka TransientCAL that minimizes issues such as sample drift and global thermal expansion, and which is also particularly convenient in calibrating nanoscale structures with size-dependent thermoreflectance. To our knowledge, our system has obtained the highest resolution calibrated temperature map of an operating plasmonic device to date.

Acknowledgments

Contributions as follows: thermoreflectance microscope and software developed by Microsanj LLC and A. Shakouri. Data collection was by G. Hohensee and E. Pek, TransientCAL analysis by D. Kendig, device thermal

modeling (Fig. 5) by Wan Kuang, and paper drafting by G. Hohensee and K. Yazawa with input from coauthors. We thank Sergei Sochava for designing the fixture for external laser coupling to drive the HAMR prototype device while under the microscope.

References

[1] Y. Won, J. Cho, D. Agonafer, M. Asheghi and K. E. Goodson, "Cooling Limits for GaN HEMT Technology," *2013 IEEE Compound Semiconductor Integrated Circuit Symposium (CSICS)*, Monterey, CA, 2013, pp. 1-5.

[2] L. Pan and D. B. Bogy, "Data storage: Heat-assisted magnetic recording," *Nat. Photon.* **3**, 189-190 (2009).

[3] D. G. Cahill, P. V. Braun, G. Chen, D. R. Clarke, S. Fan, K. E. Goodson, P. Keblinski, W. P. King, G. D. Mahan, A. Majumdar, H. J. Maris, S. R. Phillpot, E. Pop, L. Shi, "Nanoscale thermal transport. II. 2003-2012," *Appl. Phys. Rev.* **1**, 011305 (2014).

[4] R. Wilson and D. Cahill, "Anisotropic failure of Fourier theory in time-domain thermoreflectance experiments," *Nat. Comms.* **5**, 5075 (2014).

[5] C. Monachon, L. Weber, C. Dames, "Thermal Boundary Conductance: A Materials Science Perspective." *Ann. Rev. Mat. Res.* **46**, 433-463 (2016).

[6] P. Lasch, D. Naumann, "Spatial resolution in infrared microspectroscopic imaging of tissues," Biochimica et Biophysica Acta, vol. 1758, pp. 814–829, 2006.

[7] M. H. Li, J. J. Wu, Y. B. Gianchandani, "Surface micromachined polyimide scanning thermocouple probes," Journal of Microelectromechanical Systems, vol. 10, no. 1, pp. 3-9, Mar 2001.

[8] F. Menges, H. Riel, A. Stemmer, B. Gotsmann, "Nanoscale thermometry by scanning thermal microscopy," *Rev. Sci. Instrum.* **87**, 074902 (2016).

[9] G. E. Begtrup, K. G. Ray, B. M. Kessler, T. D. Yuzvinsky, H. Garcia, and Alex Zettl, "Probing Nanoscale Solids at Thermal Extremes," *Phys. Rev. Lett.* **99** 155901 (2007)

[10] R. E. Rottmayer, S. Batra, D. Buechel, W. A. Challener, J. Hohlfeld, Y. Kubota, L. Li, B.Lu, C. Mihalcea, K. Mountfield, K. Pelhos, C. Peng, T. Rausch, M. A. Seigler, D. Weller, and X. Yang, "Heat-Assisted Magnetic Recording," *IEEE Trans. Mag.* **42** (2006)

[11] W. Yan, Y. Lo, D.E. Fowler, "Heat assisted magnetic recording transducer having protective pads," US8861317 B1, 2013.

[12] N. Zhou, X. Xu, A. T. Hammack, B. C. Stipe, K. Gao, W. Scholz, E. C. Gage, "Plasmonic near-field transducer for heat-assisted magnetic recording," *Nanophotonics* **3** (3) 141-155 (2014).

[13] A. Kinkhabwala, M. Staffaroni, O. Suzer, S. Burgos, B. Stipe, "Nanoscale thermal mapping of HAMR heads using polymer imprint thermal mapping," *IEEE Transactions on Magnetics* **52** (2) (2015).

[14] M. Mecklenburg, W. A. Hubbard, E. R. White, R. Dhall, S. B. Cronin, S. Aloni, B. C. Regan, "Nanoscale temperature mapping in operating microelectronic devices," *Science* **347** (2015).

[15] M. Farzaneh, K. Maize, D. Lüerßen, J.A. Summers, P.M. Mayer, P.E. Raad, K.P. Pipe, A. Shakouri, R.J. Ram, J.A. Hudgings, "CCD-based thermoreflectance microscopy: principles and applications", Journal of Physics D: Applied Physics, Vol.42, 143001, 2009.

[16] S. D. Brorson, A. Kazeroonian, J. S. Moodera, D. W. Face, T. K. Cheng, E. P. Ippen, M. S. Dresselhaus, G. Dresselhaus, "Femtosecond room-temperature measurements of the electron-phonon coupling constant in metallic superconductors," *Phys. Rev. Lett.* **64**, 2172 (1990)

[17] G. T. Hohensee, W.-P. Hsieh, M. D. Losego, D. Cahill, "Interpreting picosecond acoustics in the case of low interface stiffness," *Rev. Sci. Instrum.* **83** (2012)

[18] K. Yazawa, D. Kendig, K. Al-hemyari, A. Shakouri, "Transient Thermal Imaging Characterization of a Die Attached Optoelectronic Device on Silicon," Proceedings of ITherm2014, Number, 2014.

[19] A. Shakouri, A. Ziabari, D. Kendig, J.-H. Bahk, Y. Xuan, P. D. Ye, K. Yazawa, and A. Shakouri1, "Stable Thermoreflectance Thermal Imaging Microscopy with Piezoelectric Position Control," Proceedings of the 32nd Semi-Therm symposium, pp. 128 – 132, Mar. 2016.

[20] S. Dilhaire, S. Grauby, and W. Claeys, "Calibration procedure for temperature measurements by thermoreflectance under high magnification conditions," Applied Physics Letters vol. 84, pp. 822, 2004.

Appendix A: edge effects from mis-registration versus global thermal expansion

We mentioned in the section on TCAT that artifacts in a TCAT map are largely driven by edge effects, which are of two sources: imperfect image registration, and global thermal expansion. Because thermoreflectance coefficients are of order 10^{-5} to 10^{-4} K^{-1}, even a sub-nanometer error in image registration will create large edge effects that overwhelm signal from sub-micron areas along the edges of reflective surfaces on the device.

To quantify this claim, we generated a simulated edge effect image based on a CCD image of our device (Fig. A1, (a)). We applied a simple 3x3 convolution matrix to generate linear fractional shifts in the CCD image along the x- and y-axes, and subtracted the original from the shifted image.

We chose the x- and y-axis shifts so that the simulated edge effects were similar in magnitude to the edge effects we observed from a high-quality, 1st generation TCAT image. As noted in Fig. 3b, the image registration in the 1st generation TCAT software was only good to ½ pixel. The real and simulated TCAT images are shown in Fig. A1 (b) and (c), respectively, and the simulated shifts were $\Delta x = +0.030$ pixel, $\Delta y = -0.006$ pixel. With 18 nm / pixel on our camera, the Δx shift is barely more than 0.5 nm. The 3x3 linear fractional shift matrix in this case was:

$$\begin{bmatrix} 0 & 0.00582 & 0.00018 \\ 0 & 0.96418 & 0.02982 \\ 0 & 0 & 0 \end{bmatrix}$$

Evidently a sub-nanometer shift, on the order of a 10th of a pixel, is enough for the steep brightness gradient along the diffraction-limited edges of metallic features to show an edge effect with magnitude 10x to 100x larger than the thermoreflectance signal. Submicron features such as the central pole (Fig. 3a-c) are completely submerged in edge effects and cannot be calibrated in TCAT.

In the latest (3rd generation, Fig. 3e) iteration of the TCAT software, image shift related edge effects are minimal, but edge effects due to global thermal expansion remain. Figure A2 shows the full TCAT image data from which Fig. 3e was taken. Edge effects are minimal near the image registration reference region (black rectangle), and are oriented outward with increasing magnitude away from the reference. When the sample heats up on the heating stage, thermal expansion extends the dimensions of components in the field of view, which causes the stretching appearance away from the pinned reference region.

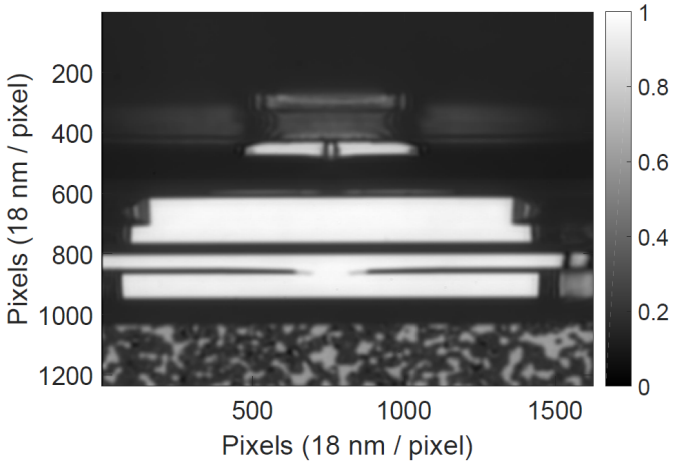

Fig. A1(a) 250x (NA = 0.9) optical CCD image of the HAMR device for the TCAT vs. simulated edge effect comparison.

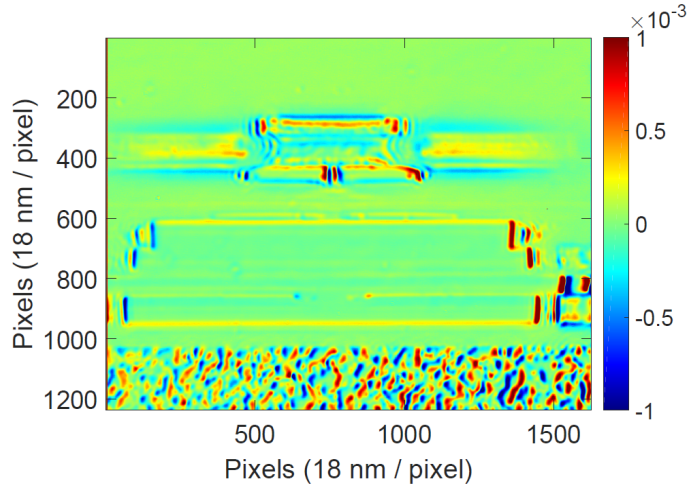

Fig. A1(b) 1st generation TCAT data, collected using 530 nm LED illumination (Thorlabs, ~15 nm FWHM), hot/cold ΔT = 23.8 K, and a 44 s hot/cold cycle period, averaging over 630 cycles. Edge effects here are largely due to flawed image registration, as can be seen in the blue/red asymmetry in left-right and top-bottom edge artifacts, as if reflective surfaces had shifted to the right.

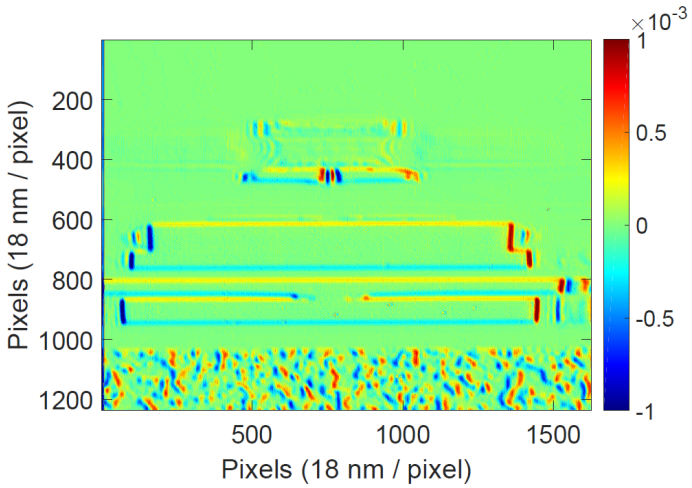

Fig. A1(c) Edge effect simulation by artificially applying Δx = +0.030 pixels, Δy = -0.006 pixels offset to the CCD image (a), and subtracting the original from the offset image.

Edge effects are minimal in the reference region, but the TCAT map does not capture the enhanced thermoreflectance along edges that we observe in our raw transient data. So we only use TCAT for the thermoreflectance coefficients of the wearpad interiors, which are unambiguous. We can then use the wearpad interiors as reference thermometers for the transient calibration technique, which addresses the thermoreflectance of diffraction-limited edges and structures.

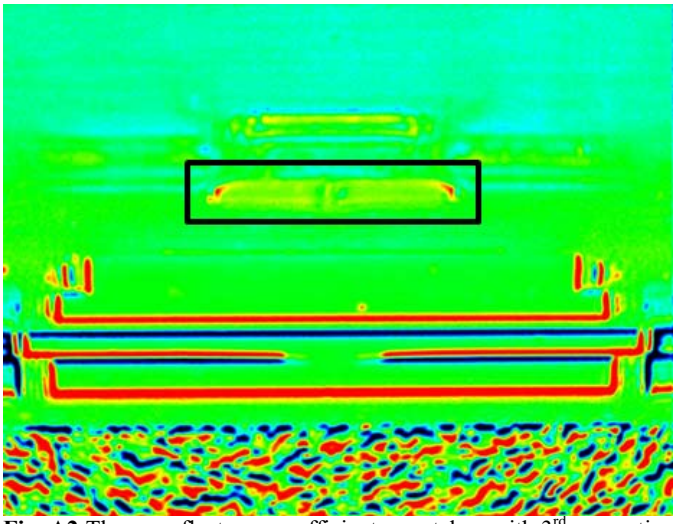

Fig. A2 Thermoreflectance coefficient map taken with 3rd generation TCAT software with subpixel image registration. Edge effects are horizontally symmetric and oriented away from the wearpad and pole device region, where the image registration reference (black rectangle) was defined. Edge effects are also more severe with increasing distance from the reference region.